

Landslides (2021) 18:2367–2381
 DOI 10.1007/s10346-021-01647-z
 Received: 1 August 2020
 Accepted: 11 January 2021
 Published online: 11 March 2021
 © The Author(s) 2021

Paolo Mazzanti · Paolo Caporossi · Alessandro Brunetti · Francesco Ismail Mohammadi ·
 Francesca Bozzano

Short-term geomorphological evolution of the Poggio Baldi landslide upper scarp via 3D change detection

Abstract On 19 March 2010, a 4 million m³ landslide occurred at Poggio Baldi, a small village in the Santa Sofia municipality, central Apennines (Forlì-Cesena, Italy). The landslide caused severe damages to some homes and obstructed both the SS310 national road and the Bidente river. The Poggio Baldi landslide arose in the “Marnoso-Arenacea Romagnola” formation composed of a pelitic-arenaceous turbiditic sequence. The landslide was classified as a rotational landslide, evolving into a partially confined flow-like landslide and causing the reactivation of the deposit of a previous landslide that took place in 1914. This paper reports a study of the phenomena currently occurring on the 100-m high main scarp of this landslide complex. The aim of the study was to assess ground changes that occurred on the upper scarp from 2015 to 2018 and to infer a preliminary evolutionary model capable of supporting short-term landslide scenarios. For this purpose, multi-station terrestrial laser scanner surveys were performed in 2015, 2016, 2017, and 2018. Additionally, an unmanned aerial vehicle three-dimensional photogrammetric survey was carried out in 2016. Analyses of the three-dimensional digital models of the main scarp made it possible to carry out several exhaustive multi-temporal investigations and to derive a detailed three-dimensional change detection scheme for it. The results showed an active geomorphological evolution of the rock scarp area due to frequent rockfalls and topples (of the order of a few m³), with significant local volume changes (a few thousand m³/year) and with potential implications for the long-term evolution of the entire slope.

Keywords UAV photogrammetry · Terrestrial laser scanner · Poggio Baldi landslide · Rockfall mapping · Volume estimation · 3D change detection

Introduction

Among different landslide types (Varnes 1978; Cruden and Varnes 1996; Hungr et al. 2014), rockfalls are the most frequent and widespread (Abellán et al. 2011; Mineo et al. 2018). In recent years, surveying and monitoring approaches have demonstrated to have great potential for rockfall hazard assessment (Miko et al. 2005; Rosser et al. 2005; Lato et al. 2009; Abellán et al. 2011; Mazzanti et al. 2015; Kromer et al. 2017a, b), in part resulting from the availability of an increasing number of remote sensing techniques (Mantovani et al. 1996; Delacourt et al. 2004; Jaboyedoff et al. 2010; Stumpf et al. 2014; Mazzanti et al. 2015). The complexity of investigating vertical cliffs (i.e. the most common source of rockfalls) by conventional field inspections can be significantly reduced by the availability of high-resolution digital terrain models (DTMs) (Delacourt et al. 2004; Bitelli et al. 2004; Dewitte et al. 2008; Yin et al. 2010; Bozzano et al. 2011; Qiao et al. 2013; Scaioni et al. 2013, 2014; Margottini et al. 2015; Bossi et al. 2015; Kromer et al. 2017a, b; Williams et al. 2018).

According to Lato et al. (2014, 2015), conventional field-based observations and analyses can be supplemented by high-resolution, remotely acquired three-dimensional (3D) data of the ground surface, obtained from different sensors and platforms, including terrestrial laser scanners (TLSs) and aerial photogrammetry (Abellán et al. 2011, 2016). Recent studies have focused on the application of either TLSs or 3D photogrammetry, although both methods can be combined as hybrid data sets to maximise spatial coverage and point density (Jaboyedoff et al. 2010; Ventura et al. 2011; Abellán et al. 2011; Niethammer et al. 2012; Lato et al. 2014, 2015; Al-Rawabdeh et al. 2016, 2017; Mineo et al. 2018). Some authors have used multi-temporal applications to investigate both the spatial and temporal evolution of some events, such as 3D change detection (CD) (Abellán et al. 2016; Barbarella et al. 2015; Esposito et al. 2017), and, in some cases, they have gained interesting insights into the geomorphological process under review (Williams et al. 2018).

This paper deals with the results of a four-year (2015–2018) monitoring activity based on multi-temporal TLS and 3D unmanned aerial vehicle (UAV) photogrammetric surveys of the rock cliff exposed by the latest reactivation of the Poggio Baldi landslide (Mazzanti et al. 2017). Subsequently, 3D CD analyses were conducted, and detailed measurements were taken of the volume changes due to the occurrence of repeated rockfalls, in order to shed light on the short-term evolution of the cliff and, on that basis, formulate assumptions about the long-term activity of the overall Poggio Baldi slope (Fig. 1).

Geological and geomorphological setting of the Poggio Baldi landslide

The landslide originated in the Forlivese Apennines, i.e. the central portion of the northern Apennines, a W-NW-ESE-oriented fold thrust belt. The upper Bidente river valley is carved within the Marnoso-Arenacea formation (Miocene), made up of pelitic-arenaceous turbidites, consisting of an alternation of claystone, siltstone, and sandstone (Ricci Lucchi 1975, 1981; Martelli et al. 2002; Conti et al. 2009).

The tectonic setting features a series of NW-SE-oriented thrust faults; as a result, the mountain ridges are composed of thrust sheets characterised by mildly folded structures, which accommodated the compressive tectonic deformation (Ricci Lucchi 1981; Farabegoli et al. 1991; Conti et al. 2009; Feroni et al. 2001; Martelli et al. 2002; Bonini 2007; Mazzanti et al. 2017).

The slope affected by the Poggio Baldi landslide is a part of the hanging wall of a major thrust system (San Benedetto in Alpe); it consists of alternating siltstone and sandstone, arranged in a homoclinal dip slope sequence (Fig. 2). A slight bending of strata panels occurs in the lower part of the slope: the bedding attitude, dipping about 45° upslope, progressively decreases, reaching dip angles of about 15–20° (Fig. 2). The structural setting is completed by a set of high-angle, normal

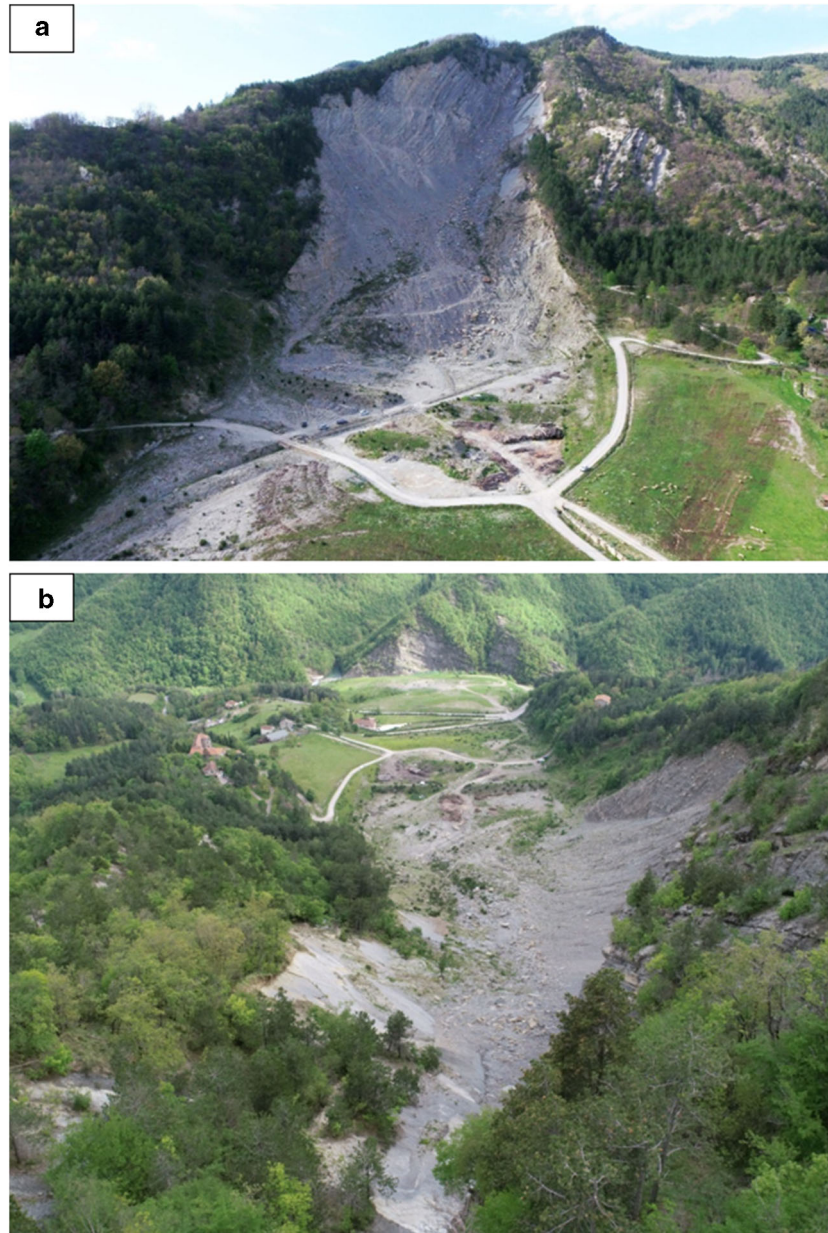


Fig. 1 UAV picture of the Poggio Baldi landslide. **a** NW view, the bedding of the “Marnoso-Arenacea” formation is clearly visible on the scarp; **b** SE view, overall slope of the Poggio Baldi landslide

faults oriented roughly perpendicular to the main thrust (Ricci Lucchi 1981; Feroni et al. 2001).

Based on stratigraphic logs from boreholes drilled immediately after the event, the maximum thickness of the landslide deposit is 42 m.

The latest reactivation of the landslide occurred between 18 and 19 March 2010, involving 4 million m³ of material. It severely damaged the SS310 national road and some buildings, reaching the Bidente valley. The Bidente river was dammed by the landslide, giving rise to an embankment of approximately 35,000 m². The landslide moved downslope in approximately three hours, after a few days of “warning signals” (e.g., opening of tension cracks), and spread over a 160,000 m² area (Mazzanti et al. 2017), with a

maximum depth of 29 m (upper sector) to 40 m (lower sector) (Benini et al. 2012; Mazzanti et al. 2017).

The 2010 Poggio Baldi landslide (Figs. 1 and 2), involving a rotational slide, can be regarded as the reactivation of a debris deposit generated by the first Poggio Baldi landslide in 1914. According to Varnes (1978) and Cruden and Varnes (1996), the 2010 landslide can be classified as a complex movement (Benini et al. 2012; Mazzanti et al. 2017). A key role in the 2010 reactivation was played by increasing water pressure due to rapid melting of snow caused by a sudden increase in temperature that occurred after a period of intense snowfall.

At present, the upper part of the slope features a sub-vertical rock cliff, with a height of up to 100 m, a width of approximately

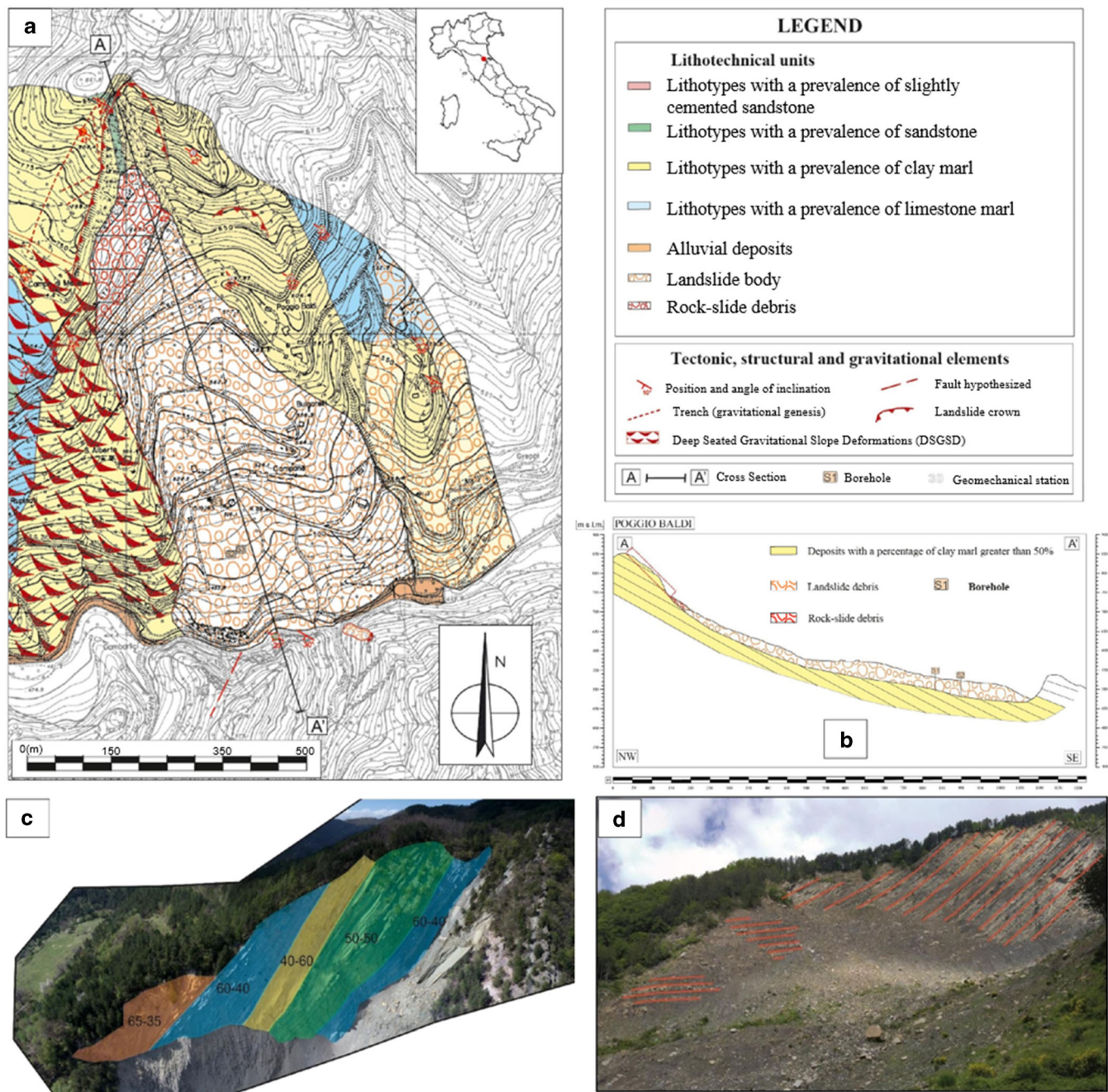


Fig. 2 a Geological map of the landslide area; b cross-section of the landslide; the dotted line shows the position of the investigated scarp; c pictures of the scarp showing different sectors with variable-ratio clay-marl/sandstone; d picture of the scarp showing different bedding inclination

250 m, and an average inclination of 70 to 90°. This sector of the slope has been experiencing frequent rockfalls and topples.

A comparison of the 1-m cell size airborne LiDAR DTM obtained after the landslide and the 1:5000 scale Regional Technical Map (CTR) built before the landslide (Benini et al. 2012) inferred height changes of - 54 m (corresponding to the vertical rock cliff zone) to + 46 m (over the landslide body before the toe).

In the past five years, there has been no evidence of movements in the landslide debris. However, in the upper part of the slope, open fractures and trenches running roughly parallel to the scarp have been identified, and frequent rockfalls and topples have

affected the main scarp, thus creating constantly growing slope debris over the main landslide debris.

Material and methods

Data collection

The Poggio Baldi landslide has been extensively investigated in recent years by a variety of remote sensing technologies and contact monitoring. The “Servizio Area Romagna” (former “Servizio Tecnico di Bacino”) of the Forlì-Cesena municipality installed a number of permanent inclinometers, piezometers, and

extensometers in the landslide area in 2010. A series of comprehensive geological and geomorphological field surveys have also been conducted in recent years. Moreover, both multi-temporal and multi-station TLS and 3D UAV photogrammetric surveys have been performed since 2015 (Mazzanti et al. 2017).

Terrestrial laser scanner surveys

The first TLS survey was carried out in April 2015 using a RIEGL VZ-1000 laser scanner equipped with a NIKON D700 12.1 MPx digital single-lens reflex (DSLR) camera with a full-frame CMOS sensor (36 × 23.9 mm) and a 20-mm fixed lens (Fig. 3). An auxiliary Global Navigation Satellite System (GNSS) survey provided a

series of reference point coordinates suitable for accurate georeferencing of TLS products.

Specifically, two permanent ground-based fixed scan positions on both sides of the landslide and six temporary scan positions were selected to provide complete coverage of the landslide and thus reduce the extent of shadow zones (Fig. 3, Table 1).

As regards permanent scan positions, use was made of an accurate repositioning system consisting of metal plates fixed to the ground, providing a ground-based platform.

The 2015 TLS survey was performed from all the selected scan positions, both permanent and temporary. In contrast, in the following years (i.e. during the monitoring period), use was made

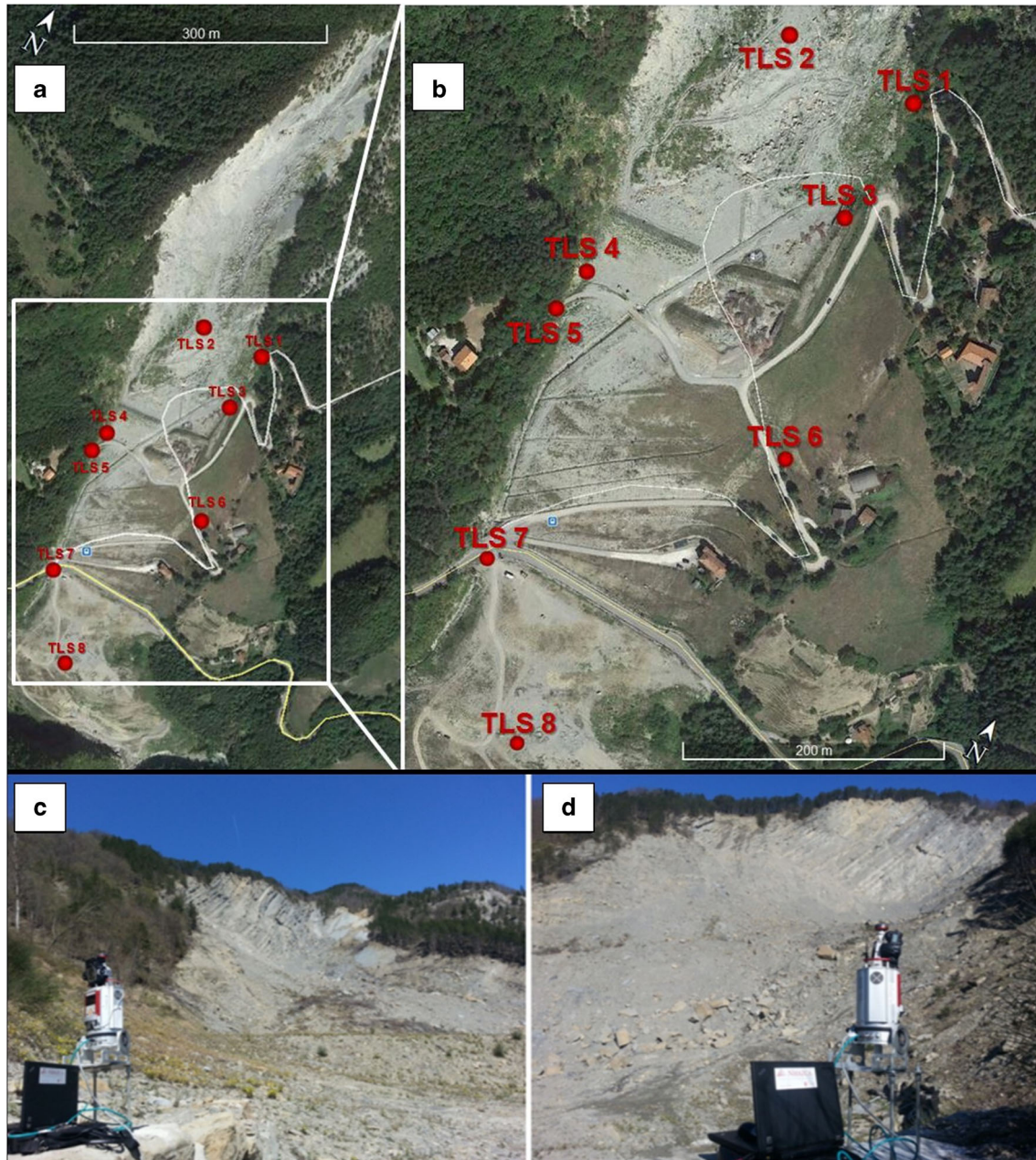


Fig. 3 Scan positions in the Poggio Baldi landslide. a Positioning along the landslide; b central portion of the landslide; c one of the left-side scan positions; and d one of the right-side scan positions. The location of the different scan positions is also reported in Table 1

Table 1 Coordinates of the scan positions selected for TLS monitoring

Scan position	Type	Coordinate reference system: UTM WGS84 32 T		Altitude [m above sea level]
		East [m]	North [m]	
TLS_1	Temporary	725,634.20	4,865,562.87	611.35
TLS_2	Temporary	725,537.93	4,865,551.45	616.74
TLS_3	Permanent	725,643.23	4,865,481.50	584.99
TLS_4	Permanent	725,511.14	4,865,354.04	580.55
TLS_5	Temporary	725,507.33	4,865,321.90	584.02
TLS_6	Temporary	725,710.84	4,865,321.12	569.34
TLS_7	Temporary	725,568.874	4,865,141.352	538.714
TLS_8	Temporary	725,671.035	4,865,028.647	521.518

As reported here, TLS_3 and TLS_4 were chosen as permanent scan positions, as they could provide a complementary view of the main scarp (frontal and lateral view, respectively)

of the permanent scan positions only, since they were considered as sufficient to fully scan the scarp. Indeed, the two permanent scan positions were selected in such a way as to obtain a complementary view of the scarp, point clouds with as few occlusions as possible, and a resolution of about 0.05 m. Furthermore, scanning from permanent platforms ensured the replicability of the geometrical acquisition scheme, thus simplifying the multi-temporal analysis of the main scarp.

Multi-temporal TLS monitoring surveys were conducted in April 2015, May 2016, May 2017, and May 2018.

UAV photogrammetric survey

A grid of 13 artificial Ground Control Points (GCPs), consisting of 35 × 35 cm white square panels with black dots at their centres, was initially installed over the central part of the Poggio Baldi landslide area at different altitudes. Then, a GNSS survey was performed using a GeoMax Zenith 25 Pro GPS/GNSS Base and an RTK Rover Station to obtain the geographic coordinates of the GCP network for georeferencing purposes.

The subsequent photogrammetric survey was performed via a DJI Phantom 4 equipped with GPS, an IMU apparatus, and a 12.4 MPx on-board camera with a 1/2.32-in. sensor size and a 20-mm lens.

The UAV photogrammetric survey was performed in April 2016. To investigate the entire landslide, three different flights were made between 1.00 PM and 3:30 PM CET, and approximately 950 images were collected. The UAV flights had been planned in such a way as to achieve the best coverage of the area of interest. Therefore, the Poggio Baldi landslide was divided into two sectors, keeping the on-board camera orientation as fixed as possible in each sector (Fig. 4, Table 2). Because of the complex orientation and topography of the slope, no satellite coverage signal was available. Hence, the UAV flights were in manual mode. An overlap of about 60–70% front-lap and 40–50% side-lap was preserved between the frames.

Data processing

Different tools were used for both TLS and 3D photogrammetric data processing, with a view to deriving 3D point clouds of the Poggio Baldi landslides. Specifically, reliance was made on the following software:

- RIEGL RiSCAN PRO v. 1.7.4: used for TLS data processing to generate the 3D point clouds derived from TLS surveys.

- Agisoft Photoscan Professional v.1.2.5 Full Demo: the UAV - collected frames were processed by using the standard Structure from Motion (SfM) workflow offered by this software and described in Westoby et al. (2012) and Smith et al. (2015) and (Agisoft 2020).
- CloudCompare® v. 2.7.0: open-source software used for comparing all the different point clouds collected.

TLS and photogrammetric point clouds were generated by using the above-described software, achieving an average point cloud density over the whole scarp of 75 points/m² for permanent TLS, 250 points/m² for multi-station TLS, and 220 points/m² for photogrammetry.

Subsequently, the point clouds were analysed, overlapped, and compared via CloudCompare® v. 2.7.0 (Girardeau-Montaut 2006). Resort was made to the M3C2 algorithm (Multiscale Model to Model Cloud Comparison), implemented in the open-source CloudCompare® v. 2.7.0 software (Girardeau-Montaut 2006), to compare pairs of multi-temporal point clouds. This algorithm does not require interpolation, but estimates the normals to the surfaces and distances directly from the point clouds (Lague et al. 2013; Stumpf et al. 2014). For CD purposes, the point clouds were first manually aligned, taking only those that had not changed in time as reference points, and then automatically refined, taking advantage of the ICP algorithm, which enabled us to remove the farthest points from the alignment process (Akca 2007). Afterwards, the point clouds were co-registered using a local coordinate system, rather than an absolute coordinate system, in order to maximise the average root mean square error (RMSE) between each aligned point cloud, thus reducing the noise in the CD results. Specifically, an average relative RMSE ranging between 2.5 mm and 10 cm for the X, Y, and Z axes was achieved for all the compared point clouds, in line with the values available in the scientific literature (e.g. Esposito et al. 2017). Further information about the M3C2 algorithm is given in Lague et al. (2013) and Barnhart and Crosby (2013). Therefore, by systematically selecting one of the two multi-temporal point clouds as a reference, the distance between the point clouds was calculated along the three axes (X, Y, and Z). In this way, a number of 3D CD analyses were performed to quantify volume changes.

For calibration, validation, and management of the retrieved DTMs and orthophotos, use was made of Geographic Information

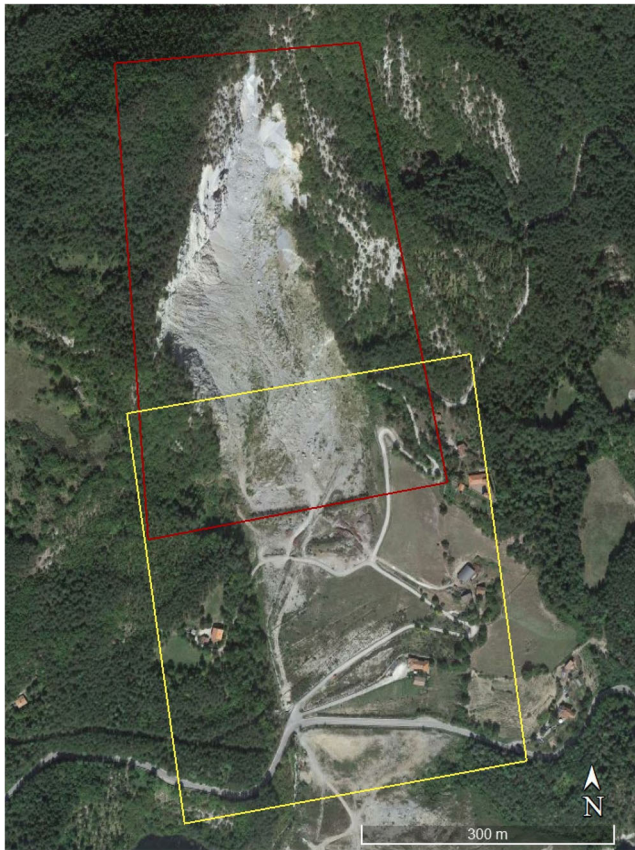


Fig. 4 For the UAV survey, the Poggio Baldi landslide was divided into two different sectors, including the main scarp, a portion of the upper landslide body (red polygon), and the central landslide body (yellow polygon)

System (GIS) software. Additional descriptions of the algorithms and tools of the above-mentioned software are available on the relevant websites.

3D change detection analyses

Three different 3D CD approaches were adopted to assess the behaviour of the investigated vertical rock cliff. In this way, both a comprehensive overview of the phenomena that occurred and the ongoing geomorphological evolution of the Poggio Baldi landslide were assessed (Fig. 5).

Several 3D CD analyses between the available 3D point clouds made it possible to investigate some specific sectors located on the main scarp and affected by significant changes.

In particular, to obtain the results discussed below, the point clouds derived from the 2015 multi-station TLS survey, the 2016 UAV photogrammetric survey, and surveys from the permanent TLS stations carried out in 2015, 2016, 2017, and 2018 were analysed.

Moreover, to validate the 3D CD results, 2015 and 2017 TLS 3D point clouds derived from permanent stations were compared with the 2016 UAV photogrammetric 3D point clouds. The comparison enabled us to identify the corresponding sectors on the main scarp of the Poggio Baldi landslide involved in debris erosion or deposition phenomena. In addition to geometric localisation of these sectors, volumes were measured in a way similar to that used for the multi-temporal TLS survey, by assessing the 3D UAV photogrammetric technique reliability. Basically, volume changes were measured with the 2.5D volume calculation algorithm embedded in CloudCompare® v. 2.7.0, which relies on rasterisation of clouds.

The relevant workflow is shown in Fig. 5.

Results

3D CD results led us to identify specific sectors undergoing significant changes since 2015. These sectors were mainly identified on the main scarp of the Poggio Baldi landslide.

3D change detection of multi-station TLS (2015) and UAV SfM 3D point clouds (2016)

As can be seen in Fig. 6, different changes can be observed in terms of both lack of material at the top of the cliff and accumulation of material, mainly at the toe of the rock cliff. By analysing the M3C2 values, and thus the lack of or accumulation of material, ranges of -1.5 to -0.9 m (difference distance decrease) and of up to $+1.1$ and $+1.5$ m (difference distance increase) were calculated.

Moreover, in the upper-left portion of the vertical rock cliff, at an elevation of approximately 700 to 750 m above sea level, a specific sector exhibited an alternation of areas with lack of and accumulation of material, arranged along a series of bulging arenaceous strata. The related 2D topographic section A–B (as reported in Fig. 6, part 1) clearly shows that a topographic change occurred between 2015 and 2016 along the maximum dip direction of the strata (Fig. 6, part 2).

3D change detection of TLS point clouds derived from permanent stations

3D CD analyses were carried out on 3D point clouds collected at fixed positions (TLS_3 and TLS_4), with a one-year temporal baseline, in order to determine similarities and changes in slope

Table 2 Details of the UAV survey of the Poggio Baldi landslide

Sector	Investigated sector	UAV flight [#]	Estimated area [ha]	Images [#]	Overlap (%)	On-board camera orientation [°]	Average flying altitude [m above sea level]
A	Main scarp and part of upper landslide body	2	11	615	60–70 front 40–50 side	90–60	20–50
B	Central landslide body	1	17	113	60–70 front 40–50 side	Nadir	70–100

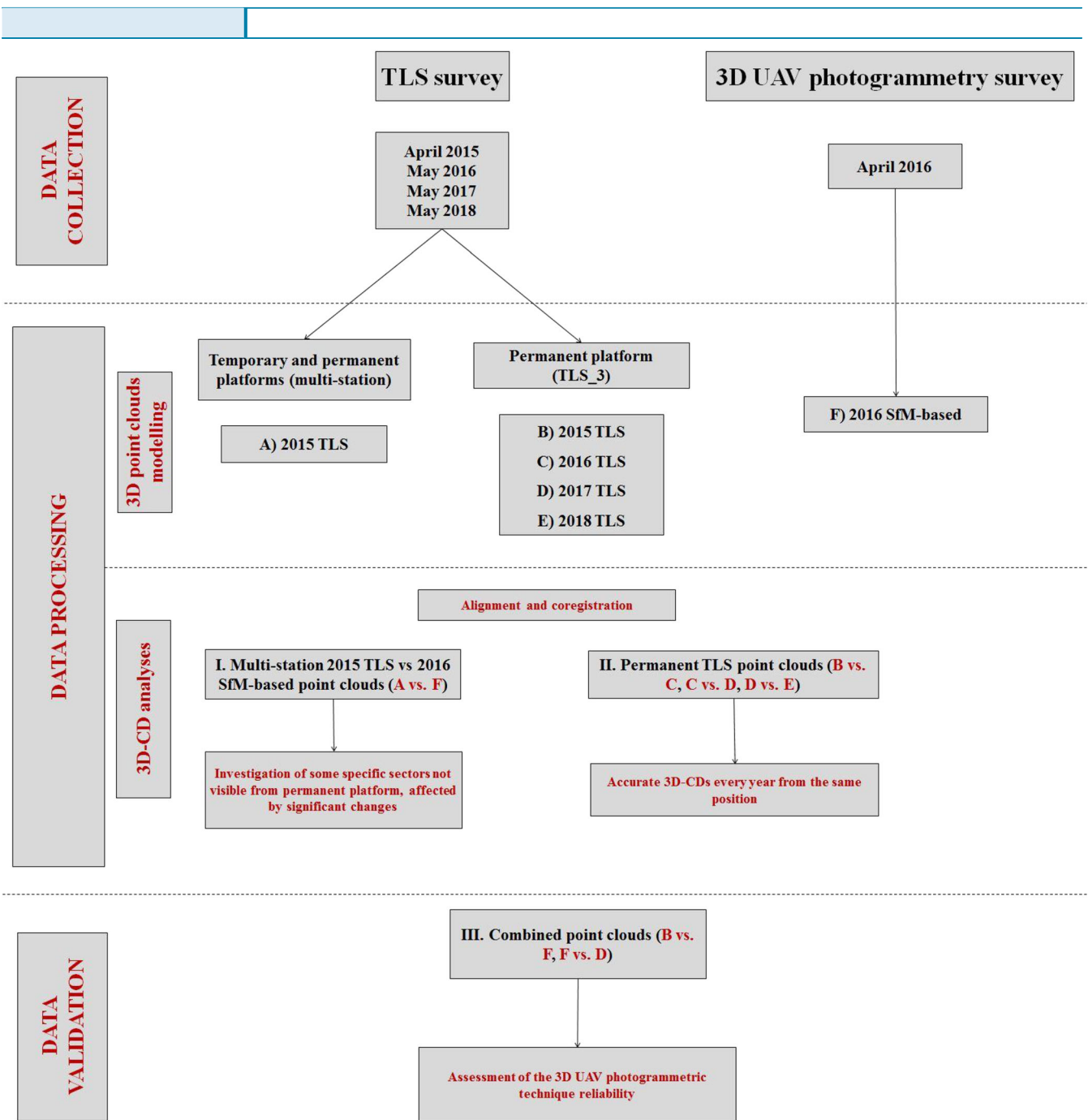


Fig. 5 Workflow of data collection and processing. 3D CD analyses were based on three different approaches, which allowed us to investigate the behaviour of the main scarp and assess the reliability of the 3D UAV photogrammetry technique

evolution over time. As reported in Fig. 7, 3D CD analyses of TLS point clouds made it possible to distinguish zones with different behaviour over time, especially in terms of depletion areas, and other zones with a similar activity. Moreover, a substantial spatial coincidence of the deposition area was observed over time, with continuous growth of material in an elongated feature at the toe of the cliff whose thickness decreased with increasing distance from the cliff.

The main ground changes were measured on the vertical rock cliff and along the upper part of the landslide deposit. Topographic

changes ranged between -3.1 and -2.2 m (depletion) and up to $+1.2$ and $+1.5$ m (deposition).

The general loss of volume that occurred in all three monitoring timespans was estimated to be in the range of 2.0 to 2.8×10^3 m³ per year (Table 3).

Validation of results

To assess the reliability and effectiveness of the 3D UAV photogrammetric technique, 3D CD analyses were also carried out between the TLS and SfM-based point clouds. The 2016 SfM-based

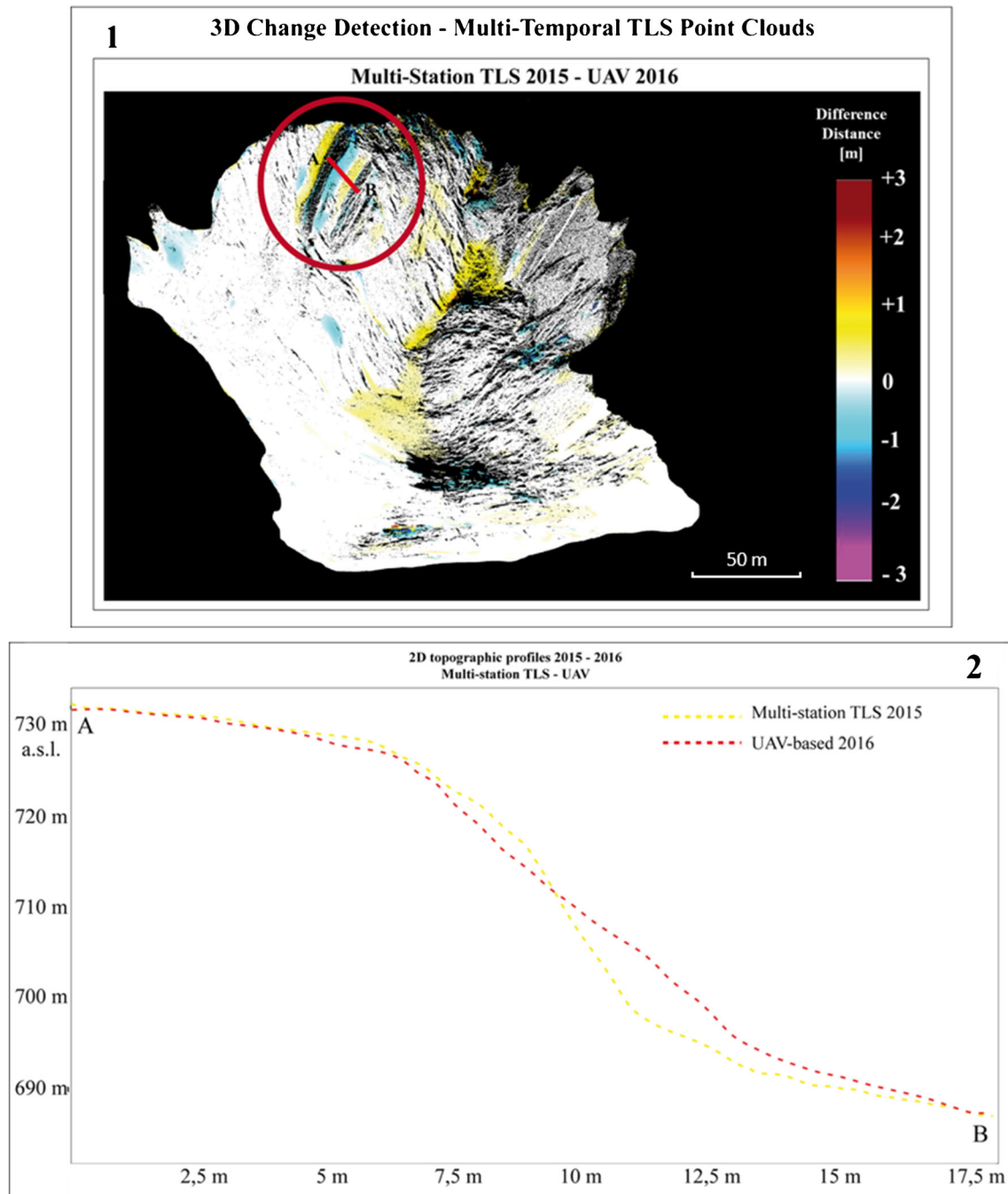


Fig. 6 3D view of the cliff showing the area affected by depletion and accumulation of material between the 2015 multi-station TLS and the 2016 SfM-based point clouds. (1) In the red circle, in the upper-left portion of the vertical rock cliff, a specific sector featured an alternation of lost and accumulated material, arranged along a series of bulging arenaceous strata. (2) 2D topographic sections built in the upper-left portion of the vertical rock cliff. The difference between the 2015 multi-station TLS (yellow line) and the 2016 UAV-based point clouds (red line) and some accumulation of material in the upper part of the cliff (owing to the presence of localised rock steps) are clearly visible

point clouds were used in combination with both 2015 and 2017 TLS point clouds taken from fixed positions. Results were compared with those obtained by TLS 3D CD analyses from fixed positions in the same timeframes and considered as a reference. Tables 4 and 5 display the volume increase/decrease of the main identified sectors affected by volume changes as obtained by both TLS vs TLS and TLS vs SfM for the 2015–2016 and 2016–2017

timeframes (Fig. 8 a and b). The tables also show the differences between volume changes (Δ volume in Tables 4 and 5) obtained with different data sets in the same timeframe. As shown, volume differences for the all the sectors are below 3% of the total volume, thus validating the reliability of results. Moreover, it is worth noting the perfect fitting of the detached volume M and the corresponding cumulated volume N (Fig. 8b, Table 5).

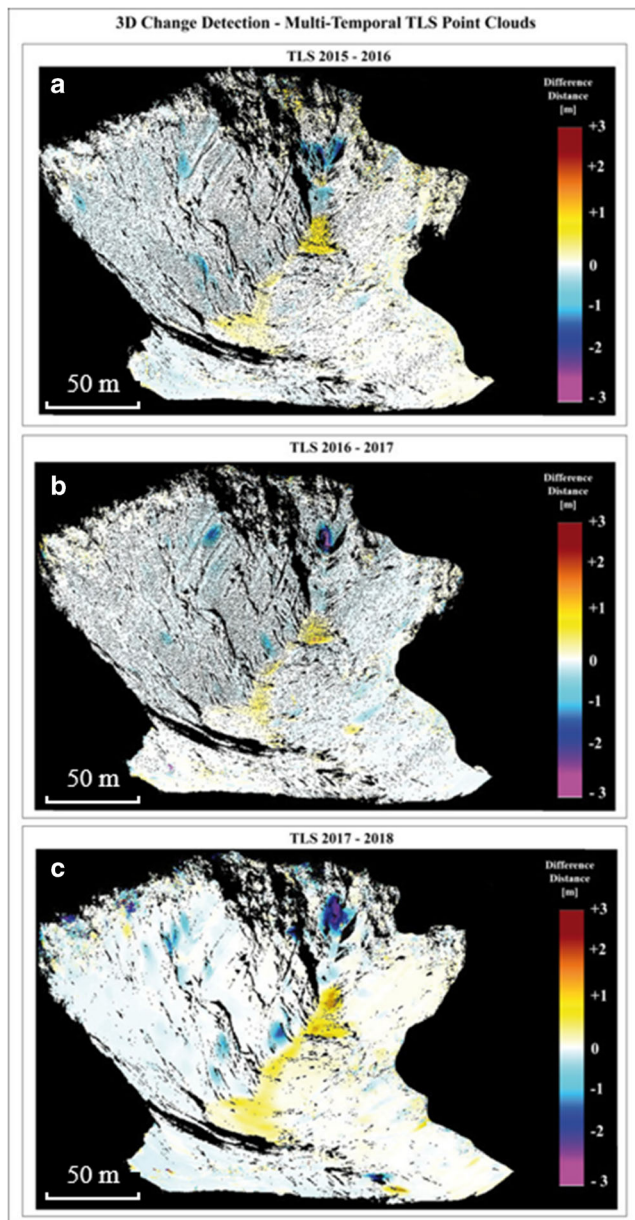


Fig. 7 Overview of the main scarp of the Poggio Baldi landslide. 3D CD analyses carried out on the available TLS point clouds between (a) 2015–2016, (b) 2016–2017, and (c) 2017–2018 point clouds are shown. Here, both negative and positive difference distance values are reported. As clearly shown, similar sectors located over the main scarp and the upper landslide body have been involved in ground changes every year since 2015

Discussion

The 3D CD analyses described above were crucial to conducting an accurate study of the geomorphological evolution of the main scarp of the Poggio Baldi landslide. This was made possible by the complementary and combined use of both TLS and SfM-based point clouds, as reported by other authors (Bitelli et al. 2004; Sturzenegger and Stead 2009; Lato et al. 2009, 2014; Wilkinson et al. 2016; Sturdivant et al. 2017; Fugazza et al. 2018; Mineo et al. 2018). The point clouds under review were generated over a timespan of four years starting from 2015. The presence of similar mobilised sectors, mainly located on the vertical rock cliff and on the upper landslide body, provides clear evidence of the state of activity of the main scarp landslide. By analysing the chronological occurrence of positive and negative values, it was possible to assess the temporal activity of the main rock scarp.

Therefore, 3D CD analyses enabled us to estimate volume changes in terms of fallen and accumulated debris and materials. Thanks to these multi-temporal analyses, a number of sectors of the rock cliff, mobilised in (i) 2015–2016, (ii) 2016–2017, and (iii) 2017–2018 (Fig. 7), were recognised. As highlighted in Fig. 9, the cumulative changes that occurred over the entire monitoring period (from 2015 to 2018) allowed us to acquire an improved understanding of the sectors of the cliff affected by recurrent phenomena with respect to those occasionally affected (i.e. detected only in one of the above-mentioned three time intervals).

Almost every year, some sectors located over the vertical rock cliff and near its toe have experienced frequent rockfalls. A large area involved in a constant loss of volume and located in the upper-central sector of the main scarp was detected in all the analyses. Here, an upward regression of the detachment zone of approximately 15–20 m was observed from 2015 to 2018. In other words, a persistent retrogressive activity of the detachment area, due to frequent rockfall events, was recorded. Additionally, a group of areas, also affected by a loss of volume, was identified near the left and upper-left portions of the main scarp. Here, rockfalls occur with daily frequency, increasing the material accumulated along the underlying areas.

As shown in Fig. 9, a wide and elongated area lying at the toe of the vertical rock cliff, at an altitude of approximately 760–630 m above sea level, was recognised. As can be seen, similar zones affected by a volume increase and covering a similar area width were identified in every gravitational instability scenario. Indeed, the main central sector of this area has been undergoing continuous processes of accumulation of fallen debris and blocks in the past four years. From those sectors, volume increases of approximately $4.4 \times 10^3 \text{ m}^3$ in 2015–2016 and of up to 2.8 and $2.9 \times 10^3 \text{ m}^3$, in both the 2016–2017 and 2017–2018 timeframes (Table 3), were estimated.

Table 3 Overview of the total volume and area changes that occurred from 2015 to 2018

Monitoring time	Volume accumulated [m ³]	Volume loss [m ³]	Δ Volume (m ³)	Area of deposition (m ²)	Area of depletion (m ²)
2015–2016	4475.8	2807.5	1668.3	3631.6	1012.1
2016–2017	2985.6	2024.7	960.9	3040.6	917.5
2017–2018	2809.9	2146.6	663.3	4031.6	492.6

Here, the surface area and volume involved in terrain variations with respect to the investigated Poggio Baldi landslide area are also reported

Table 4 Volume and area change values, both retrieved from the 3D CDs on 2015–2016 TLS data and on 2015 TLS and 2016 SfM-based data

ID [2015–2016]	Description	Measured volume [TLS vs TLS] [m ³]	Measured volume [TLS vs SfM] [m ³]	Δ Volume [m ³]	Area [TLS vs TLS] [m ²]	Area [TLS vs SfM] [m ²]	Δ area [m ²]
A	Volume increase	+ 630.5	+ 648.6	18.1	723.2	724	0.8
B	Volume decrease	– 1181.5	– 1186.6	5.1	774.4	774.1	0.3
C	Volume decrease	– 765.6	– 755.5	10.1	85.4	85.6	0.2
D	Volume decrease	– 862.3	– 865.4	3.1	152.3	153	0.7
E	Volume increase	+ 3845.3	+ 3758.6	86.7	2908.4	2907.9	0.5
F	Volume decrease	– 85.5	– 87.3	1.8	70.3	69.7	0.6
G	Volume increase	– 128.6	+ 130.7	2.1	115.6	115.9	0.3
H	Volume decrease	– 67.3	– 68.4	1.1	85.7	85.6	0.1

Considering the difference between the measured volumes, the magnitude of the accumulated volume is always larger than that of the lost volume over the entire monitored timespan (Table 3). These volume differences were 1.6×10^3 m³ (2015–2016), 9.6×10^2 m³ (2016–2017), and 6.6×10^2 m³ (2017–2018). The following factors may justify these differences: (i) the shadowing effect resulting from terrain irregularities and geometries, which had an impact on the quality of the TLS and SfM-based point clouds, especially in the upper part of the cliff and north-facing outcrops; (ii) the misdetection of small fragments that had collapsed from the source area, more visible in the deposition area; (iii) volume increase due to impact fragmentation of the material; and (iv) volume decrease due to partial removal of the fine-grained fraction of the debris mass due to runoff.

The analysis of Fig. 9 suggests that the N sector is the source of the collapsed material, which was then deposited in the M sector. The upper deposition areas appear to be thicker than the lower ones. This effect is justified by the larger dimensions of the lower deposition areas. Here, due to local morphology, the material had the opportunity to spread more than in the channelised upper portion.

Figure 10 shows the 2D topographic sections which location is reported in Fig. 9. They provide a clear overview of morphological changes taking place in these areas over time. In particular, part A of Fig. 10 shows the growth of the depositional area in the upper part of the deposition zone over the years, whereas part B shows the reduction of material caused by multiple rockfall events.

A comparative reliability study was also carried out on the role of the 3D UAV photogrammetric technique in landslide

Table 5 Comparison of volume and area changes, both retrieved from the 3D CDs on 2016–2017 TLS data and on 2016 SfM-based and 2017 TLS data

ID [2016–2017]	Description	Measured volume [TLS vs TLS] [m ³]	Measured volume [TLS vs SfM] [m ³]	Δ volume [m ³]	Area [TLS vs TLS] [m ²]	Area [TLS vs SfM] [m ²]	Δ area [m ²]
A	Volume increase	+ 398.3	+ 396.6	1.7	570.4	571.2	0.8
B	Volume decrease	– 694.6	– 687.8	6.8	485.6	484.9	0.7
I	Volume decrease	– 782.8	– 786.3	3.5	95.1	95	0.1
L	Volume decrease	– 455.6	– 462.1	6.5	117.5	118.3	0.8
E	Volume increase	+ 2498.4	+ 2447.7	50.7	2358.1	2357.9	0.2
M	Volume increase	+ 88.9	+ 88.4	0.5	112.1	111.8	0.3
N	Volume decrease	– 88.5	– 88.8	0.3	219.3	218.9	0.4

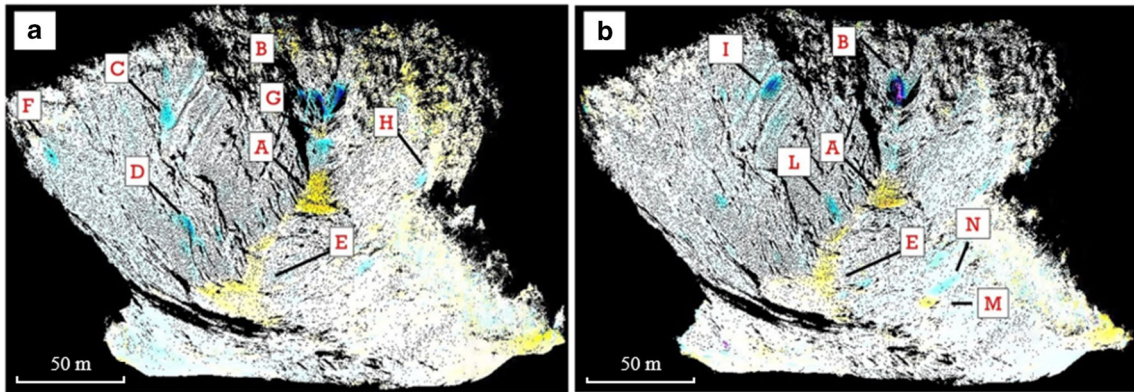


Fig. 8 Volume and area changes occurred between (a) 2015–2016 and (b) 2016–2017. Here, the TLS 3D CDs are set as a background. The relevant values are reported (following the ID order) in Tables 4 (2015–2016) and 5 (2016–2017)

monitoring activities. According to Mosbrucker et al. (2017), several factors constrain the usefulness and efficacy of SfM-derived DTMs. These factors may include scale and quality of sensors,

flight inclination, photographs, lighting and atmospheric conditions, camera calibration quality, pixel matching performance, point density, terrain and GCP characteristics and transformation,

Annual Activity - Multi-temporal TLS 3D-CD

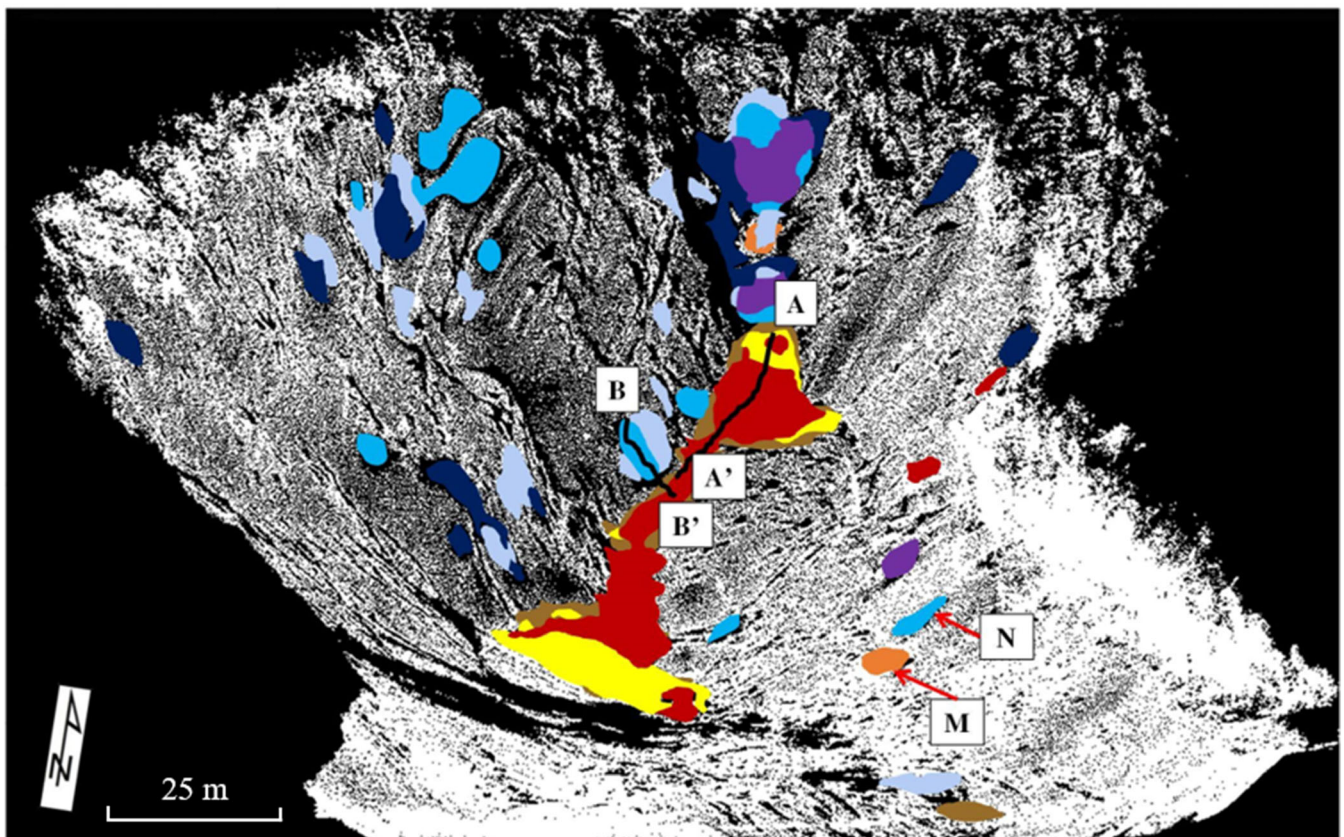


Fig. 9 Synoptic map of results achieved via multi-temporal TLS 3D CDs (from 2015 to 2018). The white colour denotes no change, while the meaning of the other colours is shown in the legend. The different colour tones identify an increase (positive) or a decrease (negative) of the volume over the years, respectively, by indicating the occurrence time of terrain changes. The terms “Positive” or “Negative” close to the colour description in the legend represent the cumulative volume increase and loss occurred between 2015 and 2018, respectively

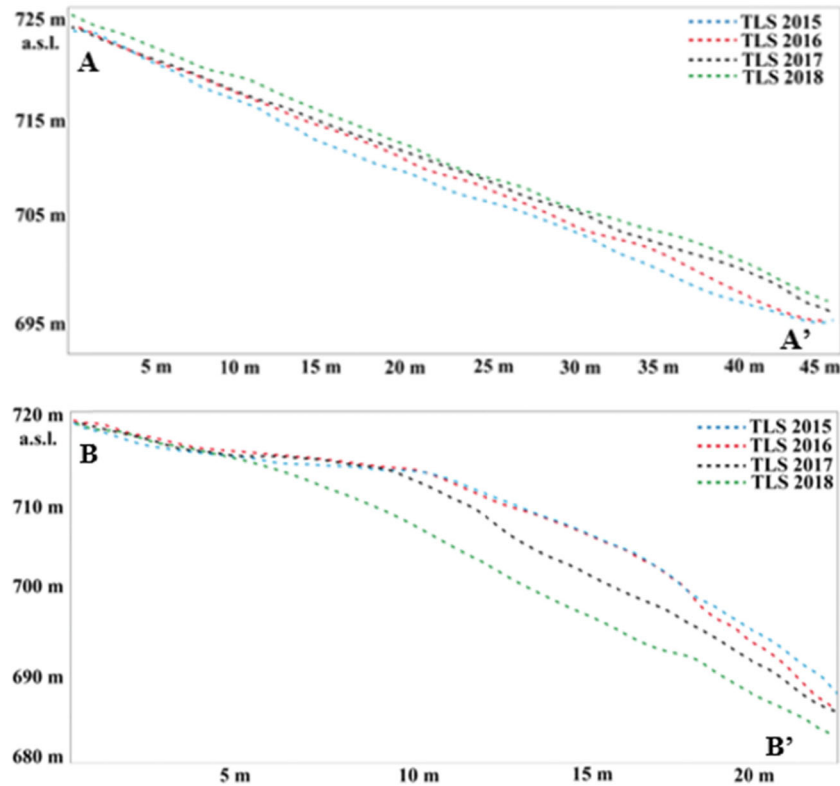


Fig. 10 Multi-temporal 2D topographic profiles (see section paths in Fig. 9)

and the DTM surface interpolation method. Although these specific factors might affect the consistency and reliability of the SfM-based DTMs, the 3D UAV photogrammetric survey carried out on the Poggio Baldi landslide enabled us to build an accurate 3D model within a reasonably short time. Indeed, the SfM-based data collection was much more rapid than the TLS one. From a logistic



Fig. 11 UAV-based overview of the sector of the vertical rock cliff involved in debris accumulation over the cantilever arenaceous strata. Here, areas with a volume increase are highlighted by red polygons

point of view, the UAV survey was easier than the TLS one (which required a more complex design of activities).

According to Scaioni et al. (2014), Barbarella et al. (2015), and Margottini et al. (2015), TLS surveys could be the simplest solution for landslide monitoring. Nonetheless, this technique could not always be applied due to physical limits. Indeed, several zones of the main scarp of the Poggio Baldi landslide had wide shadow effects, especially rock indentations or areas oriented parallel to the laser beam. The complementary use of the 3D UAV photogrammetric technique was useful for fully investigating the vertical rock cliff. Limited shadow zones, resulting from the SfM-based point clouds, were appropriately integrated with those collected by the TLS survey.

As shown in Fig. 6, deposition areas were detected near the upper-left portion of the vertical rock cliff, alternating with areas affected by volume loss. These sectors resulted in shadows in the TLS point clouds due to the laser scanner acquisition geometry. In contrast, there were no such interruptions for the SfM-based data in this study. Indeed, these are the effects of debris that fell from the upper detachment areas and accumulated over the cantilever heads of the arenaceous strata, as also observed in the 2016 UAV survey (Fig. 11).

The location and position of these detachment and deposition areas in this sector of the slope proved to be useful in characterising the geomorphological evolution of the Poggio Baldi landslide. Indeed, it is reasonable to assume that both increases and losses of volume occur with a cyclical frequency during the years. Thanks to the 3D CD survey conducted between the 2015 multi-station TLS and the 2016 SfM-based point clouds, a loss of

Evolution scenario of the vertical rock-cliff of the Poggio Baldi Landslide

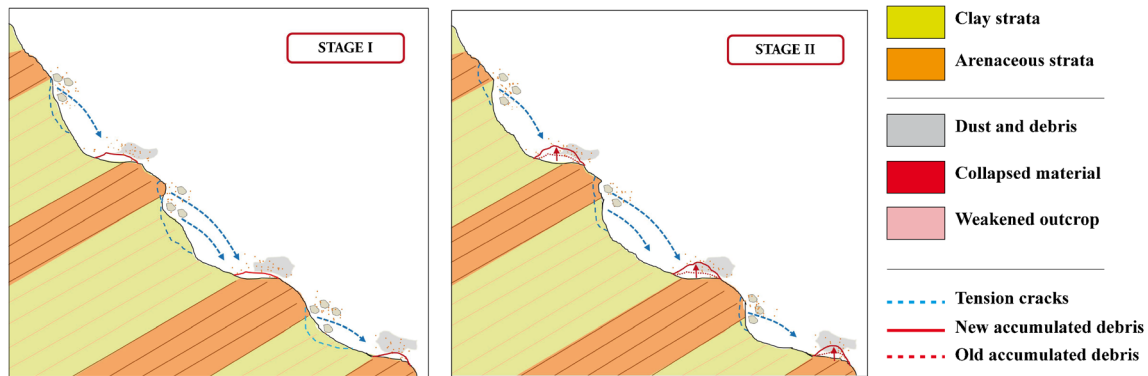


Fig. 12 Conceptual model showing the short-term evolution of the vertical rock cliff of the Poggio Baldi landslide. Here, the scale and slope angle of the strata are not respected

approximately 800–750 m³ and an accumulation of up to 600–650 m³ were recorded for this sector.

Based on the above observations, a short-term geological/geomorphological evolutionary model of the Poggio Baldi landslide (Fig. 12), based on the following two stages (STAGE I and STAGE II), was developed:

- 1 STAGE I: Slope instabilities are primarily represented by rock-falls and toppling. Predisposing factors are geological, geomorphological, and structural. The detached debris and blocks, following their own trajectories, find deposition surfaces over the cantilever arenaceous strata.
- 2 STAGE II: Over time, the volume of fallen material increases on the bulging arenaceous strata surfaces. At the same time, continuous volume loss causes a constant retrogressive activity of the above vertical rock cliff in some specific sectors. These events, repeated over time, affect the main scarp until the accumulated debris on the bulging strata surfaces, reaching non-equilibrium conditions, collapse, causing small debris avalanches.

A general annual volume depletion from the cliff ranging between 2×10^3 and 3×10^3 m³/year was recorded in all the monitoring time periods, with some recurrent detachment areas also affected by retrogressive activity and some other sectors affected by episodic activations. However, the detached material that accumulated at the toe of the cliff caused a volume increase of the debris at the toe of the scarp ranging between 4.4×10^3 m³ and 2.8×10^3 m³ per year. Assuming a constant rate of material deposition in the next 100 years (similar to the time interval between the 1914 and 2010 activations), we can compute a total amount of 300,000 m³ of accumulation in the upper part of the main landslide debris. This almost constantly increasing loading could act as one of the main predisposing factors for long-term reactivation of the Poggio Baldi main landslide.

Furthermore, if the above phenomenon were combined with an increase of pore water pressure induced by rainfall events and/or

rapid snow melting (as occurred in 2010), it could cause the reactivation of the Poggio Baldi landslide. In fact, under these conditions (huge accumulation of debris and rapid increase of pore water pressure in the debris deposit), the detachment of a large rock block from the scarp could be the last trigger of slope movement, as inferred for the 2010 landslide. In addition, earthquake-induced reactivation must be considered; even if it is not historically documented, it is nonetheless consistent with the seismo-tectonic setting of this area within the Apennine chain (as indicated in the National Seismic Hazard Map of Italy, INGV (2006)). However, more detailed analyses and computations should be carried out on the lower portion of the Poggio Baldi slope, which are beyond the scope of this study.

Conclusions

The aim of this study was to assess the changes that occurred in the upper scarp of the Poggio Baldi landslide (Emilia Romagna region, northern Italy) from 2015 to 2018 and to derive a preliminary evolutionary model capable of supporting long-term risk scenarios. For this purpose, a series of 3D CD analyses was conducted by comparing both TLS and SfM-based multi-temporal point clouds.

This approach made it possible to measure volume decreases and increases, which mainly affected the vertical rock cliff and the upper portion of the landslide body. In particular, the annual volume depletion from the cliff is between 2×10^3 and 3×10^3 m³/year, whereas the annual volume of deposition at the toe of the scarp lies between 4.4×10^3 m³ and 2.8×10^3 m³ per year. Such a loading could have major implications for the overall stability of the lower part of the slope, by acting on the already existing sliding surface related to the rotational slide at midslope, especially if this loading is associated with common triggering factors in the area, such as pore water pressure induced by rainfall events and/or rapid snow melting, and earthquakes.

With regard to the short-term activity on the slope, we developed an evolutionary model based on the results of our study and explaining the occurrence of small debris avalanches from the bulging strata in the mid part of the rock cliff. These avalanches are triggered when a certain amount of debris has accumulated on

the rock cliff top. This model can be considered appropriate for rock cliffs having similar lithological/stratigraphic conditions, and it is significant in terms of risk assessment due to the different propagation behaviour of a debris avalanche with respect to a single rockfall.

Furthermore, the use of TLS and 3D UAV photogrammetry enabled us to carry out comparative analyses and validate our results. The latter showed a very good fit, increasing our overall confidence in these fairly recent surveying technologies, which are expected to become a reference tool for rockfall investigation in the next few years.

Acknowledgements

F. Marsala, a UAV-pilot certified by ENAC (Italian Civil Aviation Authority) carried out the UAV flights. P. Lusuardi (Novateko Dizainas, Inc.) conducted the GPS survey. Special thanks are given to the municipality of Santa Sofia and to Goffredo Pini for their logistic support. We also acknowledge Giandomenico Mastrantonio for his contribution in the final revision of the paper.

Funding

Open access funding provided by Università degli Studi di Roma La Sapienza within the CRUI-CARE Agreement. This work has been supported by the Department of Earth Sciences of the University of Rome “Sapienza” (as part of the MIUR grant “Dipartimenti di Eccellenza 2018–2022”), NHAZCA S.r.l., a spin-off company of the University of Rome “Sapienza”, and the “Parco Nazionale delle Foreste Casentinesi, Monte Falterona e Campigna”.

Open Access This article is licensed under a Creative Commons Attribution 4.0 International License, which permits use, sharing, adaptation, distribution and reproduction in any medium or format, as long as you give appropriate credit to the original author(s) and the source, provide a link to the Creative Commons licence, and indicate if changes were made. The images or other third party material in this article are included in the article's Creative Commons licence, unless indicated otherwise in a credit line to the material. If material is not included in the article's Creative Commons licence and your intended use is not permitted by statutory regulation or exceeds the permitted use, you will need to obtain permission directly from the copyright holder. To view a copy of this licence, visit <http://creativecommons.org/licenses/by/4.0/>.

References

- Abellán A, Vilaplana JM, Calvet J, Garcia-Selles D, Asensio E (2011) Rockfall monitoring by Terrestrial Laser Scanning – case study of the basaltic rock face at Castellfollit de la Roca (Catalonia, Spain). *Nat Hazards Earth Syst Sci* 11:829–841. <https://doi.org/10.5194/nhess-11-829-2011>
- Abellán A, Derron MH, Jaboyedoff M (2016) Use of 3D point clouds in geohazards special issue: current challenges and future trends. *Remote Sens* 8:130. <https://doi.org/10.3390/rs8020130>
- Agisoft © PhotoScan 1.4.5. Agisoft LLC. St. Petersburg, Russia. (2020) <https://www.agisoft.com/>
- Akca D (2007) Matching of 3D surfaces and their intensities. *ISPRS J Photogramm Remote Sens* 62(2):112–121. <https://doi.org/10.1016/j.isprsjprs.2006.06.001>
- Al-Rawabdeh A, He F, Mousaa A, El-Sheimy N, Habib A (2016) Using an unmanned aerial vehicle-based digital imaging system to derive a 3D point cloud for landslide scarp recognition. *Remote Sens* 8:95. <https://doi.org/10.3390/rs8020095>
- Al-Rawabdeh A, Mousaa A, Foroutan M, El-Sheimy N, Habib A (2017) Time series UAV Image-based point clouds for landslide progression evaluation applications. *Sensors (Basel)* 17(10): 2378. <https://doi.org/10.3390/s17102378>
- Barbarella M, Fiani M, Lugli A (2015) Landslide monitoring using multitemporal terrestrial laser scanning for ground displacement analysis. *Geomatics. Natural Hazards and Risk* 6(5–7):398–418. <https://doi.org/10.1080/19475705.2013.863808>
- Barnhart TB, Crosby BT (2013) Comparing two methods of surface change detection on an evolving thermokarst using high-temporal-frequency terrestrial laser scanning, Selawik River, Alaska. *Remote Sens* 5:2813–2837. <https://doi.org/10.3390/rs5062813>
- Benini A, Biavati G, Generali M, Pizzolo M (2012) The Poggio Baldi Landslide (high Bidente valley): event and post-event analysis and geological characterization. *Proceedings 7th EUREGEO*, Volume 1, Bologna, Italy
- Bitelli G, Dubbini M, Zanutta A (2004) Terrestrial laser scanning and digital photogrammetry techniques to monitor landslide bodies. *International Archives of Photogrammetry, Remote Sensing and Spatial Information Sciences* 35(B5):246–251
- Bonini M (2007) Interrelations of mud volcanism, fluid venting, and thrust-anticline folding: examples from the external northern Apennines (Emilia-Romagna, Italy). *J Geophys Res* 112:B08413. <https://doi.org/10.1029/2006JB004859>
- Bossi G, Cavalli M, Cream S, Frigerio S, Quan Luna B, Mantovani M, Marcato G, Schenato L, Pasuto A (2015) Multi-temporal LiDAR-DTMs as a tool for modelling a complex landslide: a case study in the Rotolon catchment (eastern Italian Alps). *Nat Hazards Earth Syst Sci* 15:715–722. <https://doi.org/10.5194/nhess-15-715-2015>
- Bozzano F, Cipriani I, Mazzanti P, Prestinanzi A (2011) Displacement patterns of a landslide affected by human activities: insights from ground-based InSAR monitoring. *Natural Hazards*. DOI: 10.007/s11069-011-9840-6
- Conti P, Pieruccini P, Bonciani F, Callegari I (2009) Explanatory notes of the geological map of Italy, scale 1:50.000, sheet 266 “Mercato Saraceno”
- Cruden DM, Varnes DJ (1996) Landslide types and processes. In *Landslides: Investigation and Mitigation*; Turner, AK, Schuster, RL, Eds.; National Academy Press: Washington, DC, USA, pp 36–75
- Delacourt C, Allemand P, Casson B, Vadon H (2004) Velocity field of the “La Clapière” landslide measured by the correlation of aerial and QuickBird satellite images. *Geophys Res Lett* 31:L15619. <https://doi.org/10.1029/2004GL020193>
- Dewitte O, Jasselette JC, Cornet Y, Van Den Eeckhaut M, Collignon A, Poesen J, Demoulin A (2008) Tracking landslide displacements by multi-temporal DTMs: a combined aerial stereophotogrammetric and LiDAR approach in western Belgium. *Eng Geol* 99:11–22. <https://doi.org/10.1016/j.enggeo.2008.02.006>
- Esposito G, Mastroiocco G, Salvini R, Oliveti M, Starita P (2017) Application of UAV photogrammetry for the multi-temporal estimation of surface extent and volumetric excavation in the Sa Pigada Bianca open-pit mine, Sardinia, Italy. *Environ Earth Sci* 76:103. <https://doi.org/10.1007/s12665-017-6409-z>
- Farabegoli E, Benini A, Martelli L, Onorevoli G, Severi P (1991) Geology of the Romagna Apennines from Campigna to Cesenatico. *Mem Descr Carta Geol d'It XLVI*:165–184
- Feroni AC, Leoni L, Martelli L, Martinelli P, Ottria G, Sarti G (2001) The Romagna Apennines, Italy: an eroded duplex. *Geol J* 36:39–54. <https://doi.org/10.1002/gj.874>
- Fugazza D, Scaioni M, Corti M, D'Agata C, Azzoni RS, Cernuschi M, Smiraglia C, Diolaiuti GA (2018) Combination of UAV and terrestrial photogrammetry to assess rapid glacier evolution and map glacier hazards. *Nat Hazards Earth Syst Sci* 18:1055–1071. <https://doi.org/10.5194/nhess-18-1055-2018>
- Girardeau-Montaut D (2006) Détection de Changement sur des Données Géométriques 3D. PhD manuscript (in French), Signal and Image processing, Telecom Paris (<http://www.pastel.archives-ouvertes.fr/pastel-00001745>). Accessed on 28 February 2020
- Hungr O, Leroueil S, Picarelli L (2014) The Varnes classification of landslide types, an update. *Landslides* 11:167–194. <https://doi.org/10.1007/s10346-013-0436-y>
- INGV (2006) National Seismic Hazard Map of Italy, OPGM 3519/2006. AII. 1B
- Jaboyedoff M, Oppikofer T, Abellán A, Derron MH, Loyer A, Metzger R, Pedrazzini A (2010) Use of LiDAR in landslide investigations: a review. *Nat Hazards* 61:5–28. <https://doi.org/10.1007/s11069-010-9634-2>
- Kromer R, Lato MJ, Hutchinson DJ, Gauthier D, Edwards T (2017a) Managing rockfall risk through baseline monitoring of precursors using a terrestrial laser scanner. *Canadian Geotechnical Journal* 54(7):953–967. <https://doi.org/10.1139/cgj-2016-0178>
- Kromer RA, Abellán A, Hutchinson DJ, Lato MJ, Chanut MA, Dubois L, Jaboyedoff M (2017b) Automated terrestrial laser scanning with near real-time change detection - monitoring of the Séchillienne landslide. *Earth Surf. Dynam. Discuss.* <https://doi.org/10.5194/esurf-2017-6>
- Lague D, Brodu N, Leroux J (2013) Accurate 3D comparison of complex topography with terrestrial laser scanner: application to the Rangitikei canyon (N-Z). *ISPRS J Photogramm* 82:10–26. <https://doi.org/10.1016/j.isprsjprs.2013.04.009>

- Lato MJ, Hutchinson DJ, Diederichs M, Ball D, Harrap R (2009) Engineering monitoring of rockfall hazards along transportation corridors: using mobile terrestrial LiDAR. *Nat Hazards Earth Syst Sci* 9:935–946
- Lato MJ, Hutchinson DJ, Gauthier D, Edwards T, Ondercin M (2014) Comparison of airborne laser scanning, terrestrial laser scanning, and terrestrial photogrammetry for mapping differential slope change in mountainous terrain. *Can Geotech J* 52(2):129–140. <https://doi.org/10.1139/cgj-2014-0051>
- Lato MJ, Gauthier D, Hutchinson DJ (2015) Rock slopes asset management. Selecting the Optimal Three-Dimensional Remote Sensing Technology Transportation Research Record. *J Transp Res Board* 2510. <https://doi.org/10.3141/2510-02>
- Mantovani F, Soeters R, Van Wasten CJ (1996) Remote sensing techniques for landslide studies and hazard zonation in Europe. *Geomorphology* 15:213–225
- Margottini C, Spizzichino D, Crosta GB, Frattini P, Mazzanti P, Scarascia Mugnozza G, Beninati L. Rock fall instabilities and safety of visitors in the historic rock cut monastery of Vardzia (Georgia). Proceedings of the Volcanic Rocks and Soils Workshop. Isle of Ischia, Italy (24–25 September 2015)
- Martelli L, Camassi R, Catanzariti R, Fornaciari E, Peruzza L, Spadafora E (2002) Explanatory notes of the geological map of Italy, scale 1:50,000, sheet 265 “Bagno di Romagna”
- Mazzanti P, Brunetti A, Bretschneider A (2015) A New Approach Based on Terrestrial Remote-sensing Techniques for Rock Fall Hazard Assessment. in: *Modern technologies for landslide monitoring and prediction*, SPRINGER: 69–87.
- Mazzanti P, Bozzano F, Brunetti A, Caporossi P, Esposito C, Scarascia Mugnozza G (2017) Experimental landslide monitoring site of Poggio Baldi landslide (Santa Sofia, N-Apennine, Italy). Springer International Publishing AG M. Mikoš et al. (eds.), *Advancing Culture of Living with Landslides*, https://doi.org/10.1007/978-3-319-53487-9_29
- Miko M, Vidmar A, Brilly M (2005) Using a laser measurement system for monitoring morphological changes on the Strug rock fall, Slovenia. *Natural Hazards and Earth System Science*, Copernicus Publications on behalf of the European Geosciences Union, 5 (1): 143–153
- Mineo S, Pappalardo G, Mangiameli M, Campolo S, Mussumeci G (2018) Rockfall analysis for preliminary Hazard assessment of the cliff of Taormina Saracen Castle (Sicily). *Sustainability* 10:417. <https://doi.org/10.3390/su10020417>
- Mosbrucker AR, Major J, Spicer KR, Pitlick J (2017) Camera system considerations for geomorphic applications of SfM photogrammetry. *Earth Surf Process Landforms* 42:969–986. <https://doi.org/10.1002/esp.4066>
- Niethammer U, James MR, Rothmund S, Travelletti J, Joswig M (2012) UAV-based remote sensing of the Super-Sauze landslide: evaluation and results. *Engineering Geology* 128:2–11. <https://doi.org/10.1016/j.enggeo.2011.03.012>
- Qiao G, Lu P, Scaioni M, Xu S, Tong X, Feng T, Wu H, Chen W, Tian Y, Wang W, Li R (2013) Landslide investigation with remote sensing and sensor network: from susceptibility mapping and scaled-down simulation towards in situ sensor network design. *Remote Sens* 5:4319–4346. <https://doi.org/10.3390/rs5094319>
- Ricci Lucchi F (1975) Depositional cycles in two turbidite formations of northern Apennines. *J Sediment Petrol* 45:1–43
- Ricci Lucchi F (1981) The Miocene Marnoso-Arenacea turbidites, Romagna and Umbria Apennines. In: F. Ricci Lucchi (ed.), *Excursion Guidebook*, 2nd Eur. Reg. Meeting. Int. Ass. Sed: 229–303, Bologna
- RIEGL RiSCAN PRO v. 1.7.4. RIEGL Laser Measurement Systems GmbH. Horn, Austria (2020). <http://www.riegl.com/>
- Rosser NJ, Petley DN, Lim M, Dunning SA, Allison RJ (2005) Terrestrial laser scanning for monitoring the process of hard rock coastal cliff erosion. *Q J Eng Geol Hydrogeol* 38(4):363–375. <https://doi.org/10.1144/1470-9236/05-008>
- Scaioni M, Roncella R, Alba MI (2013) Change detection and deformation analysis in point clouds: application to rock face monitoring. *Photogramm Eng Remote Sens* 79:441–455
- Scaioni M, Longoni L, Melillo V, Papini M (2014) Remote sensing for landslide investigations: an overview of recent achievements and perspectives. *Remote Sens* 6, 1-x manuscripts. ISSN 2072-4292
- Smith MW, Carrivick JL, Quincey DJ (2015) Structure from motion photogrammetry in physical geography. *Progress in Physical Geography* 1–29. 10.1177%2F0309133315615805
- Stumpf A, Malet JP, Deseilligny MP, Skupinski G (2014) Ground-based multi-view photogrammetry for the monitoring of landslide deformation and erosion. *Geomorphology*. 231:130–145. <https://doi.org/10.1016/j.geomorph.2014.10.039>
- Sturdivant EJ, Lents EE, Thieler ER, Farris AS, Weber KM, Remsen DP, Miner S, Henderson RE (2017) UAS-SfM for coastal research: geomorphic feature extraction and land cover classification from high-resolution elevation and optical imagery. *Remote Sens* 9:1020. <https://doi.org/10.3390/rs9101020>
- Sturzenegger M, Stead D (2009) Close-range terrestrial digital photogrammetry and terrestrial laser scanning for discontinuity characterization on rock cuts. *Engineering Geology*, Volume 106:163–182. <https://doi.org/10.1016/j.enggeo.2009.03.004>
- Varnes DJ (1978) Slope movements, type and process. Schuster RL, Krizel RJ, eds., *Landslides analysis and control*. Transp. Res. Board., Special report 176, Nat. Acad. Press. Washington, D.C., 11–33
- Ventura G, Vilardo G, Terranova C, Bellucci Sessa E (2011) Tracking and evolution of complex active landslides by multi-temporal airborne LiDAR data: the Montaguto landslide (Southern Italy). *Remote Sens Environ* 115:3237–3248. <https://doi.org/10.1016/j.rse.2011.07.007>
- Westoby MJ, Brasington J, Glasser NF, Hambrey MJ, Reynolds JM (2012) ‘Structure-from-Motion’ photogrammetry: a low-cost, effective tool for geoscience applications. *Geomorphology* 179:300–314. <https://doi.org/10.1016/j.geomorph.2012.08.021>
- Wilkinson MW, Jones RR, Woods CE, Gilment SR, McCaffrey KJW, Kokkalas S, Long JJ (2016) A comparison of terrestrial laser scanning and structure-from-motion photogrammetry as methods for digital outcrop acquisition. *Geosphere* 12(6):1865–1880. <https://doi.org/10.1130/GES01342.1>
- Williams JG, Rosser NJ, Hardy RJ, Brain MJ, Afana AA (2018) Optimising 4-D surface change detection: an approach for capturing rockfall magnitude–frequency. *Earth surface dynamics* 6(1):101–119
- Yin Y, Zheng W, Liu Y, Zhang J, Li X (2010) Integration of GPS with InSAR to monitoring of the Jiayu landslide in Sichuan. *China Landslides* 7:359–365. <https://doi.org/10.1007/s10346-010-0225-9>

P. Mazzanti (✉) · **F. Bozzano**

Department of Earth Sciences, CERI Research Centre, University of Rome “Sapienza”, P.le Aldo Moro 5, 00185, Rome, Italy
Email: paolo.mazzanti@uniroma1.it

P. Mazzanti · **A. Brunetti** · **F. Bozzano**

NHAZCA S.r.l., Via Vittorio Bachelet 12, 00185, Rome, Italy

P. Caporossi

ACEA Elabori S.p.A., Engineering Geology Division, Via Vitorchiano 165, 00189, Rome, Italy

F. I. Mohammadi

IMG S.r.l. Via Cori, snc, 00177, Rome, Italy